

Single Shot Direct and Non-Line-of-Sight Imaging via Speckle Correlations

Lulu Ricketts
Carnegie Mellon University
lrickett@andrew.cmu.edu

Project Links:

[Presentation Recording Link](#)

[Link to Code](#)

Abstract

Current imaging techniques, while used widely across numerous applications with great success, encounter significant drawbacks when dealing with incoherent light sources. When light is scattered through inhomogenous media, the medium can cause random scattering of light particles that conventional camera images cannot decipher. Laser speckle photography is able to address this issue due to the memory effect of speckle correlations on diffused light. The work in this project uses direct imaging and non-line-of-sight (NLOS) imaging techniques to reconstruct objects occluded by a scattering layer by leveraging properties of speckle correlations. The experiment consists of capturing a speckle image and using speckle auto-correlation and phase-retrieval algorithms to reconstruct the object. While limited by material for ideal setup specifications, I am able to minimally reconstruct simple shapes for both direct and NLOS imaging of objects illuminated with a spatially incoherent laser source.

1. Introduction

The ability to see through visually opaque scattering media or to reconstruct occluded objects has numerous applications spanning domains such as medical imaging, autonomous vehicles and other robotics applications, military surveillance, and nanotechnology [18][17][4][9]. In the robotics domain, seeing around corners could aid mobile robots in navigating their environments by providing additional cues of their surroundings. Such work can positively impact safety in variable environments, such as those a self-driving vehicle may have to face. A previous work used a laser scanner for non line of sight imaging, but used a circular scan of the reflective surface to reconstruct the occluded 3D object illuminated by a coherent light source [8]. This project will reduce the data to a single shot image of an object illuminated with an incoherent light source through

use of an optical diffuser.

The human visual system, operating in the visible light (RGB) domain, is unable to see through visually opaque surfaces. Without a highly reflective surface like a mirror, we also cannot see objects that are not directly in our line of sight, including occluded objects around corners. Similarly, traditional RGB images, such as those captured with DSLR cameras, cannot inherently see through these occlusions either. When imaging through thin occlusions, such as biological tissues, conventional cameras result in highly distorted images, which are often times indecipherable for downstream applications. These distorted images are caused by a random scattering of light through the occluding medium, causing artifacts such as blurring or homographic distortions of the image. Therefore, these types of applications call for a different type of imaging technique.

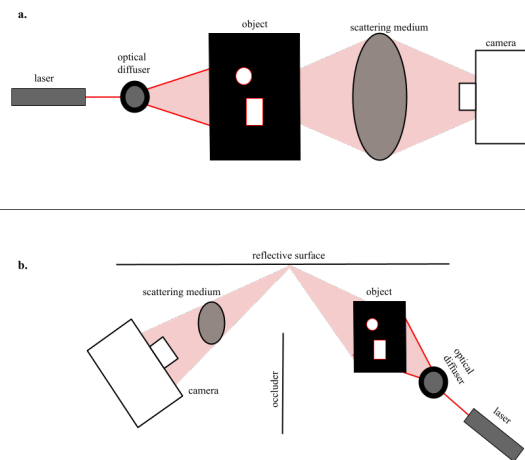


Figure 1. Schematic representation of experimental setups: (a) direct speckle imaging, a laser is passed through an optical diffuser for ensuring spatial incoherence, an object, scattering medium, and finally reaches the camera (b) non-line-of-sight (NLOS), where the wall acts as the scattering medium before the scattered light reaches the camera

1.1. Laser Speckle Imaging

Laser speckle imaging can overcome the limitations mentioned above that are present when we attempt to image an object occluded by a visually opaque scattering layer. As opposed to the physical properties of visible light which is randomly scattered when it comes in contact with the scattering medium, light emitted from a laser is much more predictable. When it comes into contact with the scattering medium, the resulting light is scattered in such a way that any shift in the laser's emission angle results in a highly correlated shifted version of itself. This property is known as the 'memory effect' of speckle photography [11][6].

Because of this effect, we can reproduce the hidden object (up to some diffraction-limited fidelity) when imaging through the surface. The high correlation between shifts in any given speckle image under this setup allows us to gain information about the scene via computing the autocorrelation of the retrieved speckle image. We can observe that the computed autocorrelation of the scene has a high similarity to the autocorrelation of the original object. From this, the final scene can be reconstructed using a phase-retrieval algorithm [13][5]. This method is in theory relatively simple, one study has even shown success with images taken from a simple phone camera [10].

1.2. Non-Line-of-Sight Imaging

Laser speckle photography can also be applied to non-line-of-sight imaging applications, where the goal is to see around corners for the occluded objects. In such setups, the laser's light is directed at a wall, which acts as the scattering medium and reflects onto an object that is occluded. The camera then captures the back-diffused light and reconstruction of the object can be performed. Traditionally, highly reflective surfaces are used for these applications, such as a white-painted wall or layered with ZnO powder [10]. In this project I use a white sheet of paper pasted to a wall.

2. Related Works

Works relating to speckle imaging correlations point to applications in the medical field, robotics, tracking occluded movement, and finding evidence of tampering. Prior to work in speckle imaging, wave-front shaping was the state of the art method in imaging through visually opaque surfaces.

Wave-front shaping: The wavefront shaping technique was one of the primary techniques that allowed imaging through highly scattering samples by constructing waves that match the scattering properties of the scattering medium. However, there exist many limitations to this technique that caused it to not be feasible in a high range of situations. These include requiring invasive imaging from both

sides of the medium, the presence of a guide star or known object, and a long acquisition time that made it difficult to collect a large number of samples over time [12].

Medical applications: Imaging the human body in the past was a highly invasive and difficult task, and speckle correlations has been used in recent studies to overcome the random scattering caused by the inhomogeneity of biological tissues. One study was able to reconstruct images through samples of chicken breast and shallot skin with high fidelity, whilst others focus directly on reconstruction of blood cells through tissue [18][10].

Tracking movement: Due to the memory effect of speckle correlations, microscopic movement can be detected from changes in speckle patterns over a series of frames taken of the same scene. Movement in one area of the scene causes a lapse in correlation, while other parts of a scene remain highly similar across time [9][16]. Extending on this method, another paper proposes a novel clustering algorithm to perform non-line-of-sight tracking of microscopic motion on multiple objects in a scene using speckle statistics and geometric properties [17].

Tampering detection: The properties of speckle correlations have also been exploited to detect minuscule changes of a surface. A paper showed that they were able to reveal fingerprints and minor deformations on objects by correlating images before and after the surface was touched [15].



Figure 2. Direct line of sight imaging setup

3. Methods

In this section, I go over the methods associated with the physical properties of laser speckle photography and the downstream software methodologies to reconstruct the occluded objects in a scene.



Figure 3. Non line of sight imaging setup

3.1. Laser Speckle Imaging

The schematic representation of the experimental setups for this project are demonstrated in Figure 1, and an image of the setup itself is shown in Figures 2 and 3. Note that these setups closely mimic those proposed in [11],[10], and [9]. Figure 1(a) represents direct speckle photography, where the laser source and camera are in line with each other and the speckle is taken from the diffused light that passes through a scattering medium. Figure 1(b) shows the schematic representation for non-line-of-sight imaging (NLOS). In this, the laser's beam reflects off of the wall and through a scattering medium before reaching the camera, which allows imaging of an object on the other side of an occluding barrier.

3.1.1 Enforcing Spatial Incoherence

The laser emits a spatially coherent light beam from the laser source. For this project, I use the Lasos DPSS laser series 50 green which emits a 532nm laser beam at 52mW.

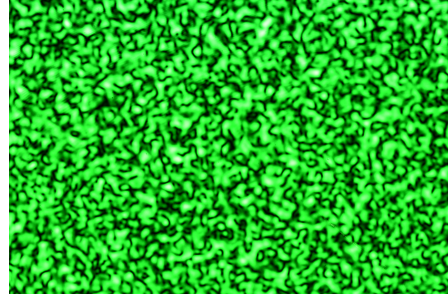


Figure 4. Camera image of a speckle pattern

This laser is fixed onto a flat surface with duct tape in line and at the same height as the camera sensor. The laser emits a beam towards the camera, or in the case of non-line-of-sight imaging, towards the reflective surface.

Spatially coherent beams, like the ones emitted by the laser, are non-optimal for computing speckle correlations. When beams emitted by the laser are spatially coherent, given two points along a wave X_1 and X_2 , they will have a high cross-correlation with one another. This leads to extreme interference between the beams when averaged over time, which in turn indicates that there is no inherent pattern of its resulting speckle pattern.

In the coming sections, we will see that it is necessary to be able to compute the autocorrelations of speckle patterns. That computation requires that the beams that resulted in the speckle were spatially incoherent and do not interfere with one another. Without spatial incoherence of the laser emission, the memory effect cannot hold for single shot imaging [6]. It may be worth noting here that some methodologies that do not require single shot imaging, and instead take and process multiple scans of the laser's emissions at multiple angles using transient sinograms, do not require this spatial incoherence assumption [8].

To enforce spatial incoherence for single shot imaging in this method, the laser's beam is first passed through an optical vibrating diffuser which reduces the noise of the signal. For this, I use the Optotune Laser Speckle Reducer LSR-3000 Series. The electro-active polymer electrodes induce oscillations of the diffuser to reduce noise, and is placed directly in front of the laser emission point.

3.1.2 Scattered Light Propagation

From the vibrating diffuser, the laser beams illuminate an object placed a couple cm away from the diffuser. The object is constructed from cutouts of a black sheet of paper that is opaque across the surface - no signal from the laser passes through - other than through the cutouts representing the 'objects.' After light passes through these objects, it hits a scattering medium that randomly scatters the light before reaching the camera sensor. For the scattering medium, a

thin napkin is used. This is held up vertically so that the beams can sufficiently pass through the medium.

As for the camera itself, I use a Nikon D3500 with a bare lens for the direct case, and maximally defocused lens for the NLOS case. It is lined up as close as possible to lie on the same horizontal plane as the laser for both direct and NLOS imaging scenarios, and for the NLOS case the camera is pointed directly at the point where the laser beam makes contact with the wall. Images are taken using variable shutter speeds for all setups (see experiments) for both scenes and a low ISO value of 100 to mitigate any noise that could be arise. The raw camera image of a speckle pattern, as shown in Figure 4, displays a seemingly uncorrelated, random speckle pattern. However, due to the memory effect arising from diffusion of spatially incoherent light, the image's autocorrelation is actually the same as the object's autocorrelation itself.

3.2. Autocorrelation

3.2.1 Memory Effect Properties

Recent work done in Bertolotti's paper [2] was one of the first to exploit the angular memory effect as it relates to speckle correlations caused by incoherent light sources. In his work, he finds that minuscule rotations $\theta = (\theta_x, \theta_y)$ of the incident light beam results in high correlated, shifted versions of the original speckle pattern. By leveraging this property, we are able to extract meaning from the seemingly random speckle patterns taken by the camera image.

However, limitations associated with the memory effect come up when the change in viewing angle $\Delta\theta$ exceeds the memory effect range. Let Δx be the distance change in a point caused by a change in $\Delta\theta$, the memory effect holds up for points lying within [10]:

$$\Delta x \ll \frac{u\lambda}{\pi L} \quad (1)$$

Here, u is the distance between the hidden object and the scattering medium, and L is the thickness of that scattering medium. Similarly, given that $\Delta\theta = \Delta x/u$, the angular field of view (FOV) is limited by:

$$\Delta\theta_{FOV} \ll \frac{\lambda}{\pi L} \quad (2)$$

Note that the memory effect ranges are inversely proportional to the thickness of the scattering medium L . In this project, we use thin scattering layers (a napkin) to attempt to increase this memory effect range. Contrastly, any increase in either the scattering medium's thickness or the distance between the scattering medium and the light source results in a decrease in the cross-correlation of the image and subsequently a decrease in the ability to reconstruct the hidden object [9][3].

3.2.2 Autocorrelation

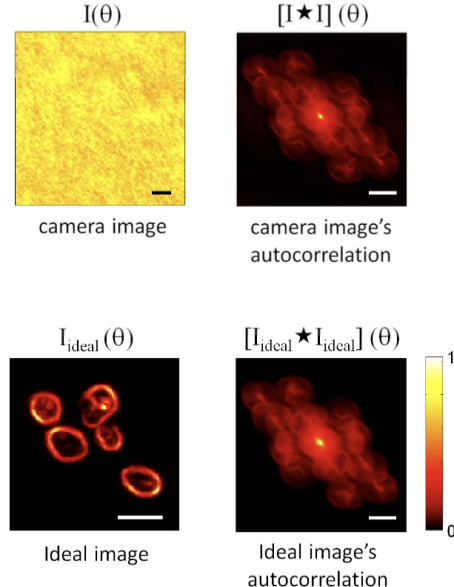


Figure 5. Image from [10], showing that the autocorrelation of camera image $I(\theta)$ is in theory highly similar to the autocorrelation of the object's intensity $O(\theta)$ (called I_{ideal} in the figure). This is due to the memory effect

Let u be the distance between the object and scattering medium, and v be the distance between the scattering medium and the camera. For angular views and points lying within the memory effect range, we can model the resulting diffused light through the scattering medium as a point spread function with magnification:

$$M = \frac{v}{u} \quad (3)$$

This allows us to define the v -weighted points on camera image I as the convolution between the u -weighted object's intensity pattern O and the speckle pattern S [10]:

$$I(v\theta) = O(u\theta) * S(\theta) \quad (4)$$

From this, we can observe that the autocorrelation of image I with itself is defined as [10][2]:

$$[I * I](\theta) = [(O * O) * (S * S)](\theta) \quad (5)$$

$$[I * I](\theta) \approx (O * O)(\theta) \quad (6)$$

Here, $(*)$ denotes the convolution operation and (\star) denotes the autocorrelation. In equation 6 we represent that

the autocorrelation of camera image I is approximately equal to the autocorrelation of the object's intensity itself. A visual example of this taken from is depicted in Figure 5, where I_{ideal} is the object's intensity. My own results are discussed later in the experiments and results sections. From equation 5 to 6 we are able to remove the autocorrelation of the speckle pattern S . Because the speckle pattern itself is inherently random broadband noise across the spatial domain, its autocorrelation is sharply peaked. Thus its convolution with any other signal results in minimal changes in the other signal.

3.3. Phase Retrieval

Phase retrieval is subsequently used to reconstruct the hidden object from the camera image's autocorrelation. Prior to running the phase retrieval algorithm, we extract the magnitudes of the autocorrelation via the absolute value of its Fourier transform, because the phase retrieval algorithm requires the pixel-wise intensities in the frequency domain in order to extract phase information. This is a difficult problem since there are a closed set of possible objects that could have resulted in this autocorrelation pattern. The general phase retrieval algorithm essentially formulates this problem as solving a minimization problem to find the closest projection y of a point x onto this set \mathbb{S} [13]:

$$\min_y \|x - y\| = \min_y d(x, \mathbb{S}) \quad (7)$$

The original reconstruction method by Gerchberg and Saxton (GS) [7], originally derived for X-ray retrieval, solves this phase retrieval by iterating back and forth between the image and Fourier domains of the image, estimating per-pixel phase from the measured magnitudes of the autocorrelation. This project utilizes a Fienup-type hybrid input-output (HIO) algorithm, which is an extension of this method [5]. While the original GS algorithm attempts to satisfy both the Fourier domain and object domain constraints, the Fienup-type algorithms work to satisfy only the Fourier domain constraints, and returns the solution once the object constraints are satisfied as well.

The hybrid input-output algorithm estimates the change in output y should relate to a change in input Δx given point t and the set of points where the output violates object-domain constraints ν as follows [5]:

$$\Delta x^k(t) = \begin{cases} 0 & t \notin \nu \\ -y^k(t) & t \in \nu \end{cases} \quad (8)$$

The next input is then calculated as:

$$x^{k+1}(t) = \begin{cases} y^k(t) & t \notin \nu \\ x^k(t) - \beta y^k(t) & t \in \nu \end{cases} \quad (9)$$

, where β is a constant value.

A theoretical limitation to the HIO algorithm is that there is no proof of convergence, which can cause reconstructions to fail. However in general, this method has been shown to outperform the GS method.

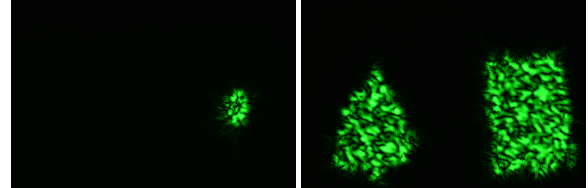


Figure 6. Objects used for imaging. On the left is an oval shape and on the object on the right contains a triangle and a rectangle. All objects are cutouts of black paper that the laser beam can illuminate through. For the two setup configurations, they are viewed from different angles (see result images below)

4. Experiments

In this project, I perform reconstruction of objects occluded by a scattering medium in two scenarios: (1) direct imaging and (2) non-line-of-sight imaging. In both these setups, I use the same two objects shown in Figure 6, which are all cutouts of a black sheet of paper that allow the laser light to go through the objects only and not their surroundings. The first is a simple oval shape about 0.2cm in diameter, and the other object contains a triangle and rectangle that are both about 0.6cm across.

The scattering medium used in all the experiments was a very thin napkin sheet, measuring about $3\mu\text{m}$ thick. I found that it was unfeasible to use anything thicker than this for the medium with the relatively large distances I had between the object, camera, and laser without completely preventing the speckle from reaching the sensor.

Images were taken with a Nikon D3500 camera at a resolution of 6000x4000 pixels. However, when processing these images for autocorrelation and phase retrieval, the images are first downsampled by a factor of 20 to decrease runtime of the algorithm. Specifically, I found that any resolution significantly greater than this resulted in `scipy.signal.correlate2d` function to freeze and not complete, even after a few hours of running.

4.1. Direct Speckle Imaging

The direct speckle imaging formulation is shown in Figures 2 and 1(a), where the laser, object, scattering medium, and camera lie on the same vertical and horizontal planes. The laser's beam travels in a straight line to the camera's sensor.

For this setup, I use a bare camera lens to take the images. The optical diffuser (ensuring spatial incoherence) is placed directly at the source of the beam within 1mm, and

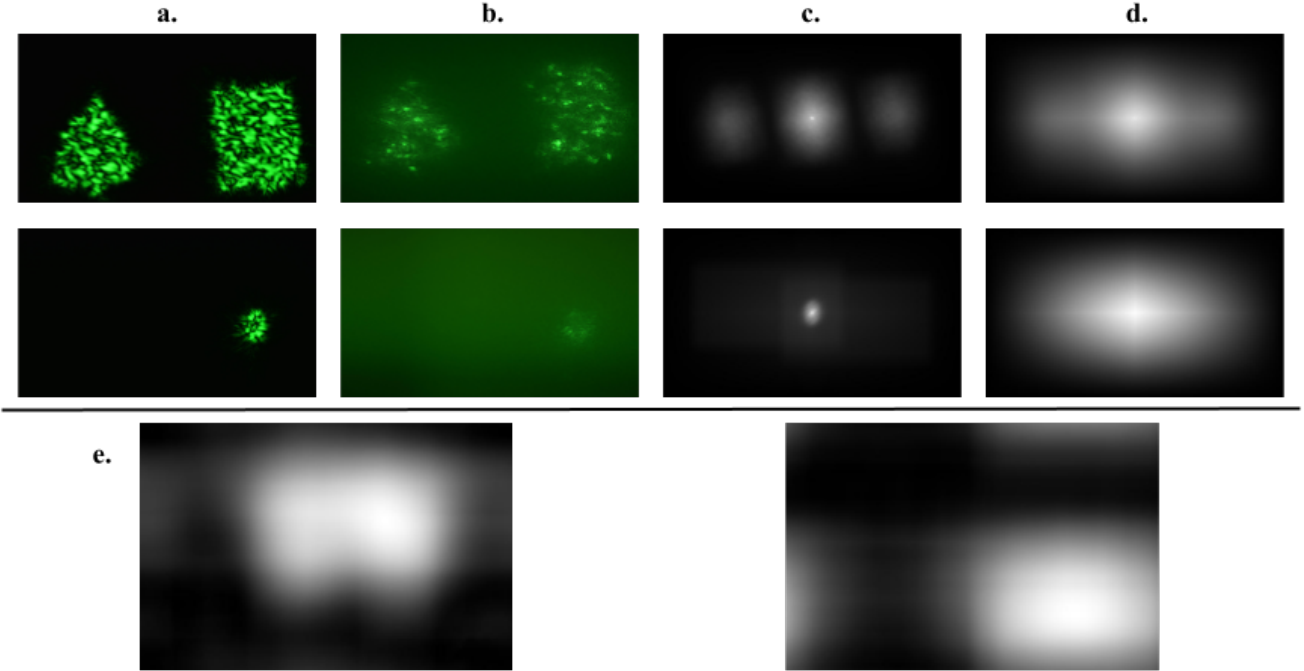


Figure 7. Results of direct line of sight imaging. Column (a) shows $O(\theta)$, the objects illuminated by the laser’s beam, which are taken with the lensless camera without a scattering medium present. Column (b) shows $I(\theta)$, the objects with a scattering medium diffusing the light across the image. (c) shows $[O * O](\theta)$ the autocorrelation of the original image in (a), and (d) shows the $[I * I](\theta)$, autocorrelation of the of the camera image in (b). The reconstruction for row 1 is shown in the left image of (e), while that of the second row is the right image.

diffuses the beam outwards toward the object. The object to be imaged is placed roughly 20cm away from the laser’s source, and the camera is 7.5cm away from that object in the opposite direction. Images are taken with ISO set to 100 for noise reduction purposes, since I allow no other light source in the scene other than the laser. Images taken with the scattering medium are taken with a shutter speed of 1/500th of a second, and 1/4000th of a second when the diffuser is not used. Unfortunately, I did not have the appropriate tools to hold up the scattering medium and had to do it by hand, so the distances were generally variable between takes. In general, I attempted to place it directly between the object and camera.

The setup configurations above were obtained after trial and error of different configurations, including changes in distances between the object, laser, and camera. I found that moving the object closer to the laser would have prevented the shape of the object from being in the camera’s scope due to the size of the objects. I was additionally constrained by the material objects used to suspend the object in the air, and thus was not able to move the camera closer to the object either.

The resulting camera images were processed with the Fienup-type phase retrieval algorithm for 300 iterations

with 30 different β values varying from [0.01, 3], and the resulting reconstructions that looked the best were chosen as the final.

4.2. Non-Line-of-Sight Speckle Imaging

The non-line-of-sight (NLOS) speckle imaging formulation is shown in Figures 3 and 1(b). As opposed to the direct imaging setup, the laser beam passes through an object and reflects off a surface (in this case, a white sheet of paper), before passing through a scattering medium and reaching the camera’s sensor. In this formulation, the images are taken with the camera lens on. The back-scattered speckle pattern from the wall proved to be too sparse for a bare camera lens to sufficiently capture.

As in the direct imaging setup, the vibrating diffuser is attached about 1mm away from the laser’s source. The object is placed 5cm from this source allowing the laser radiation to pass through. Both the object and the camera, which is perpendicularly adjacent to the laser’s beam, lie about 20cm away from the wall. The scattering medium was held roughly halfway between the camera and the wall during imaging.

I observed that the back-scattered light was much less intense in the NLOS case in comparison to the direct imaging

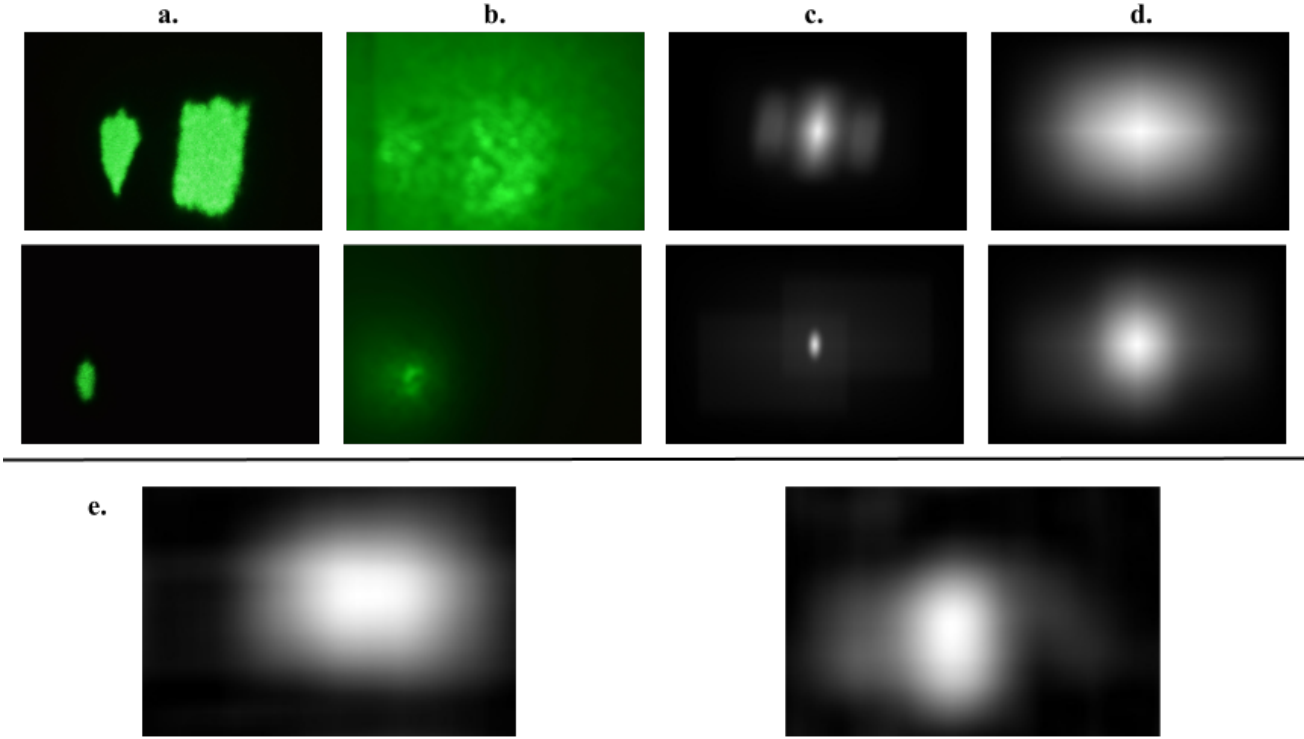


Figure 8. Results of non-line-of-sight (NLOS) imaging data and results. Column (a) shows $O(\theta)$, the objects illuminated by the laser's beam, which are taken without a scattering medium present. Column (b) shows $I(\theta)$ the objects with a scattering medium diffusing the light across the image. (c) shows $[O * O](\theta)$, the autocorrelation of the original image in (a), and (d) shows $[I * I](\theta)$, the autocorrelation of the camera image in (b). The reconstruction for row 1 is shown in the left image of (e), while that of the second row is the right image.

case. Because of this, images were taken with a longer exposure time of 5 seconds with the scattering medium, and 2 seconds without the scattering medium to produce camera images that were visible to the eye. For noise reduction purposes, the ISO was set to 100 and the smallest possible aperture (F36) was used. Furthermore, the camera was set to be extremely defocused in order to generalize the speckle patterns and further reduce any noise.

This experimental setup was processed the same as the previous section, where the Fienup-type HIO algorithm was ran for 300 iterations with varying β values ranging from [0.01, 30]. For all the experiments mentioned in this section, I had also varied number of iterations in intervals of 250 in the range [250, 3000], but found that the number of iterations did not have a significant effect on the reconstruction results, even when varying β values. Thus, I decided to limit number of iterations to 300 for all subsequent runs in order to reduce computational runtime.

5. Results

For this section, I will refer to the object containing a rectangle and triangle as **object1**, and the object containing the oval shape as **object2**.

The images, their autocorrelations, and reconstructions of the two objects associated with direct line of sight imaging are depicted in Figure 7. The reconstruction for **object1** is shown on the left side of Fig.7(e). This was generated with $\beta = 0.64$, which produced the closest reconstruction to the original image. The reconstruction for **object2** is shown on the right side of that figure and was produced using $\beta = 1.58$.

Similarly, the results for NLOS imaging are shown in Figure 8. The original objects here look blurrier than before due to the defocusing of the lens, whereas the direct line of sight setup had used a lensless camera. **Object1**'s reconstruction is shown on the left side of Fig.8(e) and was generated with $\beta = 1.74$; **object2**'s reconstruction is on the right side of the figure and was generated using $\beta = 2.37$.

6. Discussion

6.1. Analysis of Results

In general, the reconstructions obtained by the Fienup-type HIO phase retrieval method turned out blurry and did not contain perfect representations of the original images. This is a result of large relative distances between the camera and object v and between the object and laser u . As a result, the memory effect range is much smaller, even though I use a thin scattering layer L .

However, they did not completely fail either. For each of the direct and NLOS imaging cases, one of the objects resulted in reconstructions that produced the generally correct shape.

For the direct line of sight imaging setup, we see that **object2** produces a rectangular reconstruction, which is not similar to the original image. However, **object1** seems to perform better. Though the reconstruction is blurry, we can see that the algorithm is able to distinguish what looks like two shapes next to each other. Additionally, we can get an idea of the performance from the autocorrelation results. The autocorrelation of the original image I , shown in Fig.7(c)'s first row has one peak in the middle and two smaller ones on either side. In column (d)'s first row, the same pattern of peaks exist, though with some noise and activation between them as well.

In the NLOS imaging case, **object2**'s reconstruction outperforms that of **object1**. Again, we can observe that the autocorrelations in Fig.8(c,d) have the same type of oval shape that is extended farther in the vertical dimension. The final reconstruction shown on the right side of Fig.8(e) shows the same oval shape as the original image in the same general location.

The cases that did well could have been attributed to the way the light had scattered in those cases. When the speckle pattern is uniform across the entire image, the reconstructions seem to perform more poorly than if they are concentrated in and around the objects themselves. Operating under the memory effect assumption, this should not occur since the diffused light should scatter to produce the same autocorrelation pattern even when the speckles cover the entire image plane. Thus this gives evidence to this setup exceeding the range of the memory effect.

6.2. Limitations

A number of limitations were encountered in the setup and runtime of algorithms in this project.

In terms of setup, previous works had significantly smaller distances u and v between the laser, object, and imaging sensor, on the order of a couple μm or mm and rarely reaching scales as large as cm [2][3][11][14][9]. Because I constructed the setup outside of a lab that may have contained the necessary materials for achieving this level of

closeness, I was unable to replicate these distance scales in my own setup. This extended to the size of the objects themselves, which are no larger than 3mm in most other works. With a lack of appropriate tools, objects in my setup were closer to $20\text{-}60\text{mm}$ in scale.

Several consequences arose from this home setup limitation. First, I had to hold the scattering medium while taking the image. Though I held it as still as possible, microscopic movements could have distorted the speckle patterns in the image. Second, the memory effect may not have held up for these larger distances, causing autocorrelations to not have the intended patterns. Additionally, in the NLOS setup, the white paper I used was not the most optimal for back-scattering light, and surfaces such as ZnO powder could have produced more useful speckle patterns [10].

In addition, computational resources were also limiting, especially for the extremely costly autocorrelation operation which required me to downsample the camera images significantly.

6.3. Additional Work

Averaging Autocorrelations: As explained in [10], a method to both reduce noise and improve autocorrelation results is to take multiple images and average their autocorrelations. This helps account for minuscule shifts in speckle patterns that may occur.

Synthetic Speckle Rendering: One possible way to overcome some of the limitations described above could be to synthetically render speckle patterns using methods such as those described in [1]. This could eliminate the need for a setup that ensures closeness, and this paper instead uses a Monte Carlo framework to render speckles in a statistically correct way, including quantifying the memory effect.

Additional Imaging Schematics: An extension to the imaging techniques presented in this project, some works perform another version of NLOS imaging where the camera and laser are co-located with one another [17][14]. They then record an occluded 3D object from the back-scattered diffused light.

7. Acknowledgements

Huge thanks to the Computational Photography course staff, specifically Ioannis Gkioulekas and Dorian Chan, for their advisement on this project and for lending the necessary hardware.

References

- [1] Chen Bar, Marina Alterman, Ioannis Gkioulekas, and Anat Levin. A monte carlo framework for rendering speckle statistics in scattering media. *ACM Transactions on Graphics (TOG)*, 38(4):1–22, 2019. 8

- [2] Jacopo Bertolotti, Elbert G Van Putten, Christian Blum, Ad Lagendijk, Willem L Vos, and Allard P Mosk. Non-invasive imaging through opaque scattering layers. *Nature*, 491(7423):232–234, 2012. 4, 8
- [3] Kunihiko Ehira, Ryoichi Horisaki, Yohei Nishizaki, Makoto Naruse, and Jun Tanida. Spectral speckle-correlation imaging. *Applied Optics*, 60(8):2388–2392, 2021. 4, 8
- [4] Daiki Endo, Takahiro Kono, Yoshikazu Koike, Jun Yamada, and Uma Maheswari Rajagopalan. Laser speckle imaging in discrimination of zooplanktons from supermicroplastics. *Environmental Nanotechnology, Monitoring & Management*, 16:100587, 2021. 1
- [5] James R Fienup. Phase retrieval algorithms: a comparison. *Applied optics*, 21(15):2758–2769, 1982. 2, 5
- [6] Isaac Freund, Michael Rosenbluh, and Shechao Feng. Memory effects in propagation of optical waves through disordered media. *Physical review letters*, 61(20):2328, 1988. 2, 3
- [7] Ralph W Gerchberg. A practical algorithm for the determination of plane from image and diffraction pictures. *Optik*, 35(2):237–246, 1972. 5
- [8] Mariko Isogawa, Dorian Chan, Ye Yuan, Kris Kitani, and Matthew O’Toole. Efficient non-line-of-sight imaging from transient sinograms. In *European Conference on Computer Vision*, pages 193–208. Springer, 2020. 1, 3
- [9] Y Jauregui-Sánchez, Harry Penketh, and Jacopo Bertolotti. Tracking moving objects through scattering media via speckle correlations. *arXiv preprint arXiv:2202.10804*, 2022. 1, 2, 3, 4, 8
- [10] O Katz, P Heidmann, M Fink, and S Gigan. Non-invasive real-time imaging through scattering layers and around corners via speckle correlations. *Nature photonics*. 2, 3, 4, 8
- [11] Ori Katz, Eran Small, and Yaron Silberberg. Looking through walls and around corners with incoherent light: Wide-field real-time imaging through scattering media. *arXiv preprint arXiv:1202.2078*, 2012. 2, 3, 8
- [12] Allard P Mosk, Ad Lagendijk, Geoffroy Lerosey, and Matthias Fink. Controlling waves in space and time for imaging and focusing in complex media. *Nature photonics*, 6(5):283–292, 2012. 2
- [13] Eliyahu Osherovich. Numerical methods for phase retrieval. *arXiv preprint arXiv:1203.4756*, 2012. 2, 5
- [14] Adithya Pedireddla, Akshat Dave, and Ashok Veeraraghavan. Snlos: Non-line-of-sight scanning through temporal focusing. In *2019 IEEE International Conference on Computational Photography (ICCP)*, pages 1–13. IEEE, 2019. 8
- [15] Yi Chang Shih, Abe Davis, Samuel W Hasinoff, Frédo Durand, and William T Freeman. Laser speckle photography for surface tampering detection. In *2012 IEEE Conference on Computer Vision and Pattern Recognition*, pages 33–40. IEEE, 2012. 2
- [16] Brandon M Smith, Pratham Desai, Vishal Agarwal, and Mohit Gupta. Colux: Multi-object 3d micro-motion analysis using speckle imaging. *ACM Transactions on Graphics (TOG)*, 36(4):1–12, 2017. 2
- [17] Brandon M Smith, Matthew O’Toole, and Mohit Gupta. Tracking multiple objects outside the line of sight using speckle imaging. In *Proceedings of the IEEE Conference on Computer Vision and Pattern Recognition*, pages 6258–6266, 2018. 1, 2, 8
- [18] Xin Yang, Ye Pu, and Demetri Psaltis. Imaging blood cells through scattering biological tissue using speckle scanning microscopy. *Optics express*, 22(3):3405–3413, 2014. 1, 2